AIAA JOURNAL
Vol. 31, No. 1, January 1993

Flexure-Torsion Behavior of Prismatic Beams, Part I: Section Properties via Power Series

J. B. Kosmatka*
University of California, San Diego, La Jolla, California 92093

The behavior of a tip-loaded cantilever beam with an arbitrary cross section is studied using Saint-Venant's semi-inverse method along with a power series solution for the out-of-plane flexure and torsion warping functions. The power series coefficients are determined by solving a set of variationally derived linear algebraic equations. For complex cross sections, the calculated coefficients represent a "best-fit approximation" to the exact warping function. The resulting warping functions are used to determine the cross-sectional properties (torsion constant, shear correction factors, shear deformation coefficients, and shear center location). A new linear relation is developed for locating the shear center, where the twist rate is zero about the line of shear centers. Moreover, the kinematic relations for a new fully compatible one-dimensional beam theory are developed. Numerical results are presented first to verify the approach and second to provide section data on NACA four-series airfoils not currently found in the literature.

Introduction

CLOSED-FORM solutions for Saint-Venant's flexure and torsion problems (tip-loaded cantilever beam) exist for only a few simple cross-sectional shapes (ellipse, rectangle, equilateral triangle).[1-3] For general cross-sectional shapes (i.e., cambered airfoils), the cross-sectional dependent flexure and torsion warping functions cannot be determined exactly, and thus approximate techniques must be used. One proven approach for approximately determining the Saint-Venant torsion[4] and flexure[5] functions involves the application of the finite element method. In this approach, the general cross section is discretized into triangular and/or quadrilateral subregions (elements) with out-of-plane nodal variables that represent the cross-sectional warping, where the warping distribution is determined by applying the principle of minimum potential energy. Although the finite element approach is well behaved, it has two shortcomings. First, a large number of elements are required for complex cross sections, which leads to a large set of linear algebraic equations. Second, the resulting array of calculated nodal values provides very little physical insight into the warping definition, and one typically resorts to graphical finite element post processing techniques to understand the warping distribution. An alternative approach, which has been developed by Mindlin[6] for the solution of Saint-Venant's torsion problem (generalized plane strain), involves assuming a double power series for the warping function. The power series coefficients are determined by solving a set of linear algebraic equations, where the number of equations is equal to the number of unknown coefficients. Thus, the problem size is independent of the cross-sectional complexity, and only dependent on the number of terms in the power series.

The objective of the current investigation is to study the flexure and torsion behavior of a tip-loaded cantilever beam with an arbitrary cross section, where both the flexure and torsion warping functions are expressed as a double power series in terms of the cross-sectional coordinates. The coefficients associated with the power series terms are determined by solving a set of variationally derived linear algebraic equations, where the number of equations is equal to the number of unknown coefficients. For complex cross sections, the calculated coefficients represent a "best-fit approximation" to the exact warping function, which may be an infinite series of transcendental functions. To aid in the evaluation of the power series weighted area integrals, the cross section is discretized into a series of triangular subregions, where the integration in each subregion is evaluated exactly using Gaussian Quadrature formulas for triangles.[7,8] The triangle aspect ratio is not critical as opposed to the finite element method, since the power series is a global cross-sectional function and not a local element function.

Once the flexure and torsion warping functions are known for a given cross section and material definition (Poisson's ratio), then the resulting three-dimensional displacement and stress distributions can be used to 1) study the overall beam behavior; 2) determine important beam-type section properties, including the torsion constant, shear deformation coefficients, shear center location, and shear correction factors (for Timoshenko's beam theory[9,10]; and 3) develop a one-dimensional beam theory[11] that includes cross-section flexure and torsion warping effects and is fully compatible with the three-dimensional stress and displacements predictions of Saint-Venant.

The determination of the shear center location has been studied by numerous researchers,[2,3,5,12-15] where the shear center is commonly defined as "the load point where the mean value of the local cross-sectional twist is zero (i.e., local twist rate about the section centroid is zero)." Applying this definition to Saint-Venant's flexure and torsion problems leads to a zero twist rate about the centroidal axis, but any other line parallel to the centroidal axis, including the line of shear centers, will have a nonzero twist rate. This nonzero twist rate for all lines except the centroidal axis occurs because the application of a transverse tip load produces a linearly increasing bending stress state normal to the cross section and straining within the cross section. This straining within the cross section, which causes the particles of the cross section to translate and rotate into an anticlastic surface, also increases linearly from the beam tip. Thus any line that is composed of cross-sectional particles that are offset from the centroidal axis will undergo linearly varying twist (i.e., constant twist rate with zero twist at the beam tip) as a result of an applied transverse tip load. Recently, an analytical approach[16,17] was developed for locating the shear center in thin platelike cross sections, where the aforementioned definition was modified to be "the load point where the twist rate about the line of shear

Received July 29, 1991; revision received June 18, 1992; accepted for publication June 20, 1992.

*Associate Professor, Department of Applied Mechanics and Engineering Sciences. Member AIAA.

centers is zero." Although the two definitions appear to be very similar, this definition insures that the shear center is coincident with the center of twist. Moreover, numerical results for thin triangular cross sections revealed profound differences (40–67% depending on Poisson ratio) in the shear center locations. In my current paper, the shear center location is determined using both the classical definition and the more recent definition,[16,17] where a linear relationship between the two locations is developed that is valid for any cross-sectional shape and material definition.

Numerical results are presented to verify the approach and provide new data for NACA four-series airfoils. The sensitivity of the section properties (especially the shear center location) with airfoil thickness and camber is of interest to aeroelasticians because of the profound effect these parameters have on divergence and flutter speed calculations. The current work significantly improves on the fundamental studies of the shear center location for solid airfoils,[15,18] where these analyses approximately treated cambered airfoils as cubic ovals.

Theoretical Background

General Beam Behavior

We begin by considering a cantilever prismatic beam of length L with an arbitrary cross-section of area A composed of a homogeneous, isotropic material. A Cartesian coordinate system (x, y, z) with corresponding displacement components (u, v, w) is defined with the origin at the centroid of the root end, and the (x, y) axes coincide with the principal axes of the root cross section. See Fig. 1. The beam is subjected to a force with flexure components P_x and P_y that act through the centroid of the tip cross section $(z = L)$ in the x and y directions, respectively, and an applied torque M_z, where they satisfy the following three equations of stress equilibrium:

$$P_x = \int_A \tau_{xz}\, dA \tag{1a}$$

$$P_y = \int_A \tau_{yz}\, dA \tag{1b}$$

$$M_z = \int_A (x\tau_{yz} - y\tau_{xz})\, dA \tag{1c}$$

Furthermore, the body forces are considered negligible so that the in-plane stresses σ_{xx}, σ_{yy}, and τ_{xy} are equal to zero and the normal stress is defined as a linear function, following Saint-Venant's assumptions,[1-3]

$$\sigma_{zz} = \left(\frac{P_x}{I_{yy}}x + \frac{P_y}{I_{xx}}y\right)(z - L) \tag{2}$$

where I_{xx} and I_{yy} represent the principal moments of inertia about the x and y axes, respectively. Introducing these assumptions into the stress equilibrium equations and integrating yields the well-known form[1-3] of the displacement components and shear stresses

$$u = \frac{P_x}{EI_{yy}}\left[\frac{L}{2}z^2 - \frac{z^3}{6} + \frac{\nu}{2}(x^2 - y^2)(L - z)\right] + \frac{P_y}{EI_{xx}}[\nu xy(L - z)] - \theta yz + b_4 z - b_6 y + b_1 \tag{3a}$$

$$v = \frac{P_y}{EI_{xx}}\left[\frac{L}{2}z^2 - \frac{z^3}{6} + \frac{\nu}{2}(y^2 - x^2)(L - z)\right] + \frac{P_x}{EI_{yy}}[\nu xy(L - z)] + \theta xz + b_5 z + b_6 x + b_2 \tag{3b}$$

$$w = -\frac{P_x}{EI_{yy}}\left[x\left(Lz - \frac{z^2}{2}\right)\right] - \frac{P_y}{EI_{xx}}\left[y\left(Lz - \frac{z^2}{2}\right)\right] + \psi(x, y) - b_4 x - b_5 y + b_3 \tag{3c}$$

$$\tau_{yz} = -\frac{GP_x}{EI_{yy}}(\nu xy) - \frac{GP_y}{EI_{xx}}\left[\frac{\nu}{2}(y^2 - x^2)\right] + G\left(\frac{\partial\psi}{\partial y} + x\theta\right) \tag{3d}$$

$$\tau_{xz} = -\frac{GP_x}{EI_{yy}}\left[\frac{\nu}{2}(x^2 - y^2)\right] - \frac{GP_y}{EI_{xx}}(\nu xy) + G\left(\frac{\partial\psi}{\partial x} - y\theta\right) \tag{3e}$$

where E is the Young's modulus of the material, ν is the Poisson's ratio, G is the shear modulus that satisfies $\{ = E/[2(1 + \nu)]\}$, θ is the beam twist rate about the centroidal axis, $\psi(x, y)$ is a function that describes warping out of the cross-sectional plane, and b_1–b_6 are integration constants that are specified by defining the fixity of the beam root. In the current development, the geometric boundary conditions are prescribed by restraining the translational motion of the root centroid $(x = y = z = 0)$ and requiring that the slope and twist of the centroidal axis are zero at the beam root,

$$u = v = w = \frac{\partial u}{\partial z} = \frac{\partial v}{\partial z} = \frac{\partial u}{\partial y} - \frac{\partial v}{\partial x} = 0 \tag{4a-4f}$$

This approach is identical to that of Refs. 2 and 3 and thus $b_i = 0$ $(i = 1\text{-}6)$.

The determination of the warping function ψ is accomplished by applying the principle of minimum potential energy

$$\delta\Pi = \delta U - \delta W_e = 0 \tag{5a}$$

where δU is the variation of the strain energy given by

$$\delta U = \int_0^L \int_A \sigma_{zz}\delta\epsilon_{zz} + \tau_{yz}\delta\gamma_{yz} + \tau_{xz}\delta\gamma_{xz}\, dA\, dz \tag{5b}$$

since $\sigma_{xx} = \sigma_{yy} = \tau_{xy} = 0$, and δW_e is the variation of the work of external forces that results from the applied tractions on the beam ends,

$$\delta W_e = \int_A [\sigma_{zz}|_{(z=L)} - \sigma_{zz}|_{(z=0)}]\delta\psi\, dA = \frac{P_x L}{I_{yy}}\int_A x\delta\psi\, dA + \frac{P_y L}{I_{xx}}\int_A y\,\delta\psi\, dA \tag{5c}$$

Substituting Eqs. (2), (3), (5b), and (5c) into Eq. (5a) and carrying out the integration over the beam length

$$\delta\Pi = 0 = GL\int_A \frac{\partial(\delta\psi)}{\partial x}\left\{\frac{\partial\psi}{\partial x} - y\theta - \frac{P_x}{EI_{yy}}\left[\frac{\nu}{2}(x^2 - y^2)\right] - \frac{P_y}{EI_{xx}}(\nu xy)\right\} + \frac{\partial(\delta\psi)}{\partial y}\left\{\frac{\partial\psi}{\partial y} + x\theta - \frac{P_x}{EI_{yy}}(\nu xy) - \frac{P_y}{EI_{xx}}\left[\frac{\nu}{2}(y^2 - x^2)\right]\right\} dA - \frac{P_x}{EI_{yy}}EL\int_A x\delta\psi\, dA - \frac{P_y}{EI_{xx}}EL\int_A dA \tag{6}$$

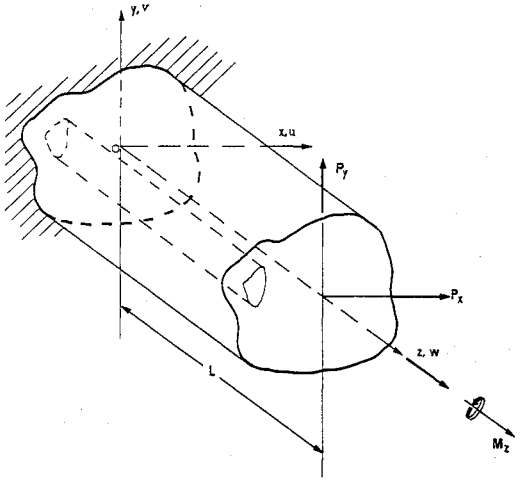

Fig. 1 Prismatic cantilever beam.

An examination of Eq. (6) reveals that ψ can be expressed as a linear combination of three cross-sectional dependent functions that are proportional to the rates of beam curvature and twist

$$\psi(x, y) = \psi_1(x, y)\frac{P_x}{EI_{yy}} + \psi_2(x, y)\frac{P_y}{EI_{xx}} + \psi_3(x, y)\theta \tag{7}$$

where ψ_1 and ψ_2 represent the shear-dependent warping functions and ψ_3 is the Saint-Venant torsion warping function.

The shear stress distributions of Eqs. (3d) and (3e) can be expressed in terms of the rates of bending curvature and twist by making use of Eq. (7),

$$\tau_{yz} = \tau_{yz_{(1)}}\frac{P_x}{EI_{yy}} + \tau_{yz_{(2)}}\frac{P_y}{EI_{xx}} + \tau_{yz_{(3)}}\theta \tag{8a}$$

$$\tau_{xz} = \tau_{xz_{(1)}}\frac{P_x}{EI_{yy}} + \tau_{xz_{(2)}}\frac{P_y}{EI_{xx}} + \tau_{xz_{(3)}}\theta \tag{8b}$$

where

$$\tau_{yz_{(1)}} = G\left(\frac{\partial\psi_1}{\partial y} - \nu xy\right) \tag{8c}$$

$$\tau_{xz_{(1)}} = G\left[\frac{\partial\psi_1}{\partial x} - \frac{\nu}{2}(x^2 - y^2)\right] \tag{8d}$$

$$\tau_{yz_{(2)}} = G\left[\frac{\partial\psi_2}{\partial y} - \frac{\nu}{2}(y^2 - x^2)\right] \tag{8e}$$

$$\tau_{xz_{(2)}} = G\left(\frac{\partial\psi_2}{\partial x} - \nu xy\right) \tag{8f}$$

$$\tau_{yz_{(3)}} = G\left(\frac{\partial\psi_3}{\partial y} + x\right) \tag{8g}$$

$$\tau_{xz_{(3)}} = G\left(\frac{\partial\psi_3}{\partial x} - y\right) \tag{8h}$$

The twist rate θ as a function of the applied loads P_x, P_y, and M_z can now be determined by substituting Eqs. (8a–8h) into Eq. (1c), integrating, and rearranging

$$\theta = \frac{1}{a_3}\left(M_z - a_1\frac{P_x}{EI_{yy}} - a_2\frac{P_x}{EI_{yy}}\right) \tag{9a}$$

where

$$a_i = \int_A x\tau_{yz_{(i)}} - y\tau_{xz_{(i)}}\, dA, \qquad (i = 1, 3) \tag{9b}$$

Torsional Rigidity and Shear Center Location

The cross-sectional torsional rigidity GJ is commonly defined as the constant a_3 in Eq. (9a). The remaining two constants a_1 and a_2 in Eq. (9a) can be used to locate the classical definition of the shear center (x_s, y_s); "the load point that produces a zero mean value cross-sectional twist" (i.e., zero local twist about section centroid, $\theta = 0$).[2,3,5,12-15] This location can be determined by applying a general flexural force (P_{xs}, P_{ys}) through the unknown point (x_s, y_s), recognizing the equivalent centroidal forces and moments are

$$P_x = P_{xs} \tag{10a}$$

$$P_y = P_{ys} \tag{10b}$$

$$M_z = P_{ys}x_s - P_{xs}y_s \tag{10c}$$

substituting these resultants into Eq. (9a), rearranging, noting that $\theta = 0$, and then

$$x_s = \frac{a_2}{EI_{xx}} \tag{10d}$$

$$y_s = -\frac{a_1}{EI_{yy}} \tag{10e}$$

Although this definition leads to a zero twist rate about the line of centroids, there will be a nonzero twist rate about every other line parallel to the centroidal axis as a result of the formation of the anticlastic surface. This is observed by calculating the micromolar twist rate as

$$\frac{\partial\omega_z}{\partial z} = \frac{1}{2}\left(\frac{\partial\gamma_{yz}}{\partial x} - \frac{\partial\gamma_{xz}}{\partial y}\right) = \theta - \frac{P_x}{EI_{yy}}(\nu y) + \frac{P_y}{EI_{xx}}(\nu x) \tag{11}$$

Applying a force (P_{xs}, P_{ys}) through the previous shear center definition will produce a zero micromolar twist rate about the centroid axis (since $x = y = \theta = 0$) but a nonzero micromolar twist rate θ_s about the calculated line of shear centers (x_s, y_s) that is equal to

$$\left.\frac{\partial\omega_z}{\partial z}\right|_{\substack{x = x_s \\ y = y_s}} = \theta_s = -\frac{P_{xs}}{EI_{yy}}(\nu y_s) + \frac{P_{ys}}{EI_{xx}}(\nu x_s) \tag{12}$$

This nonzero micromolar twist rate is illustrated in Fig. 2a, where the deformed root ($z = 0$) and tip ($z = L$) cross sections of the loaded (P_{ys}) cantilever beam are superimposed.

An alternate shear center location (x_s^*, y_s^*) can also be determined so that the application of an applied flexure force (P_{xs}, P_{ys}) will produce a zero twist rate about the calculated line of shear centers and insure that the shear center is coincident with the center of twist. The current model has advantages over the procedure of Refs. 16 and 17 in that it uses the Saint-Venant results directly and can be applied to any arbitrary cross section, not just thin cross sections. This calculation involves finding the load point in the cross-sectional plane that will produce a twist rate about the centroidal axis that is equal to the negative of the anticlastically produced micromolar twist rate, thus

$$\theta = -\theta_s^* = \frac{P_{xs}}{EI_{yy}}(\nu y_s^*) - \frac{P_{ys}}{EI_{xx}}(\nu x_s^*) \tag{13}$$

where these twist rates offset each other to produce a zero twist rate about the line of shear centers. See Fig. 2b. Substituting Eqs. (13) and (10a–10c) into Eq. (9a), one can determine this shear center location as

$$x_s^* = \frac{a_2}{(EI_{xx} + \nu GJ)} \tag{14a}$$

$$y_s^* = -\frac{a_1}{(EI_{yy} + \nu GJ)} \tag{14b}$$

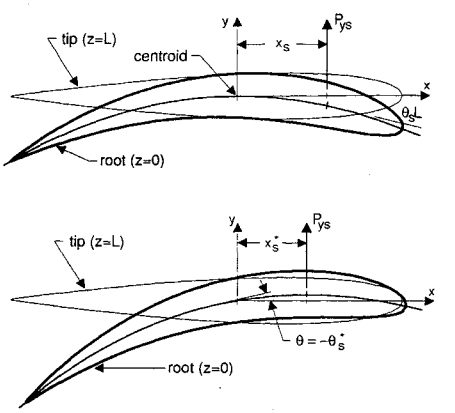

Fig. 2 Tip (—) and root (—) cross-sectional planforms of a tip-loaded P_{ys} cantilever beam with an airfoil cross section where a) zero twist about the centroidal axis and b) zero twist rate about the calculated line of shear centers.

or in terms of the previous (classical) definition by making use of Eqs. (10d) and (10e) and $G/E = \frac{1}{2}(1+\nu)$:

$$x_s^* = \frac{x_s}{1 + [\nu/(1+\nu)](J/2I_{xx})} \tag{14c}$$

$$y_s^* = \frac{y_s}{1 + [\nu/(1+\nu)](J/2I_{yy})} \tag{14d}$$

and the percent difference between the two locations can be expressed as

$$\frac{x_s - x_s^*}{x_s^*} = \frac{\nu}{(1+\nu)} \frac{J}{2I_{xx}} \tag{14e}$$

$$\frac{y_s - y_s^*}{y_s^*} = \frac{\nu}{(1+\nu)} \frac{J}{2I_{yy}} \tag{14f}$$

It is interesting to note that (x_s^*, y_s^*) will always be less than or equal to (x_s, y_s), where the two locations are equal when either the Poisson's ratio is zero, the shear center is coincident with the centroid ($a_2 = a_3 = 0$), or the cross section is very thick so that (J/I_{xx}) or (J/I_{yy}) is effectively zero. For most thin solid cross sections (including NACA airfoils or triangles), $J/I_{xx} \approx 4$, and thus the percent difference when measured from the centroid will generally vary from 40 to 67% depending on the Poisson ratio (assuming $0.25 < \nu < 0.50$), which is in agreement with the work of Refs. 16 and 17.

Shear Deformation

An examination of the displacement components of Eqs. (3a–3c) reveals that the calculated centroidal tip displacements $[u(x=y=0,\ z=L) = P_x L^3/3EI_{yy},\ v(x=y=0,\ z=L) = P_y L^3/3EI_{xx}]$ agree with the strength of materials solution, but the additional displacement associated with shear deformation does not appear as a result of our original assumption [Eqs. (4a–4f)] that the slope of the deformed centroidal axis at the beam root is zero ($b_4,\ b_5 = 0$). This additional displacement can be included by simply rotating the deformed beam so that the slope of the deformed cross section at the centroid ($x = y = 0$) is coincident with the x-y plane, and thus the deformed centroidal axis will have a nonzero slope (see Ref. 3 for additional details). The rotation angles are equal to the shear strains γ_{xz} and γ_{yz} at the centroid of the beam root ($x = y = z = 0$) and thus by combining Eqs. (3), (7), (9a), and (10), the shear angles defined in terms of the applied forces P_x, P_y, and M_z are

$$b_4 = \gamma_{xz_{(0)}} = \left(\left.\frac{\partial \psi_1}{\partial x}\right|_{x=y=0} + y_s \frac{EI_{yy}}{GJ} \left.\frac{\partial \psi_3}{\partial x}\right|_{x=y=0}\right)\frac{P_x}{EI_{yy}}$$

$$+\left(\left.\frac{\partial \psi_2}{\partial x}\right|_{x=y=0} - x_s \frac{EI_{xx}}{GJ} \left.\frac{\partial \psi_3}{\partial x}\right|_{x=y=0}\right)\frac{P_y}{EI_{xx}} + \left.\frac{\partial \psi_3}{\partial x}\right|_{x=y=0} \frac{M_z}{GJ} \tag{15a}$$

$$b_5 = \gamma_{yz_{(0)}} = \left(\left.\frac{\partial \psi_1}{\partial y}\right|_{x=y=0} + y_s \frac{EI_{yy}}{GJ} \left.\frac{\partial \psi_3}{\partial y}\right|_{x=y=0}\right)\frac{P_x}{EI_{yy}}$$

$$+\left(\left.\frac{\partial \psi_2}{\partial y}\right|_{x=y=0} - x_s \frac{EI_{xx}}{GJ} \left.\frac{\partial \psi_3}{\partial y}\right|_{x=y=0}\right)\frac{P_y}{EI_{xx}} + \left.\frac{\partial \psi_3}{\partial y}\right|_{x=y=0} \frac{M_z}{GJ} \tag{15b}$$

where the subscript 0 is introduced to symbolize the evaluation of the function at the centroid ($x = y = 0$). The final form of the displacement components, including shear deformation [from Eqs. (3a–3c)], is

$$u = \frac{P_x}{EI_{yy}}\left[\frac{L}{2}z^2 - \frac{z^3}{6} + \frac{\nu}{2}(x^2 - y^2)(L - z)\right]$$

$$+\frac{P_y}{EI_{xx}}[\nu xy(L-z)] - \theta yz + b_4 z \tag{16a}$$

$$v = \frac{P_y}{EI_{xx}}\left[\frac{L}{2}z^2 - \frac{z^3}{6} + \frac{\nu}{2}(y^2 - x^2)(L - z)\right]$$

$$+\frac{P_x}{EI_{yy}}[\nu xy(L-z)] + \theta xz + b_5 z \tag{16b}$$

$$w = -\frac{P_x}{EI_{yy}}\left[x\left(Lz - \frac{z^2}{2}\right)\right] - \frac{P_y}{EI_{xx}}\left[y\left(Lz - \frac{z^2}{2}\right)\right]$$

$$+\psi(x, y) - b_4 x - b_5 y \tag{16c}$$

where ψ, θ, b_4, and b_5 are defined in Eqs. (7), (9a), (15a), and (15b), respectively.

Kinematics of a Compatible One-Dimensional Theory

A fully compatible one-dimensional beam theory can be developed using the following kinematic relations:

$$u(x, y, z) = U(z) - y\Theta(z) + \psi_x(x, y) \tag{17a}$$

$$v(x, y, z) = V(z) + x\Theta(z) + \psi_y(x, y) \tag{17b}$$

$$w(x, y, z) = W(z) - x\Phi_y(z) + \psi_z(x, y) \tag{17c}$$

where (U, V, and W) are z-dependent displacement functions that act along the x, y, and z directions, respectively; Φ_x, Φ_y, and Θ are z-dependent rotations about the x, y, and z axes, respectively; and ψ_x, ψ_y, and ψ_z represent cross-sectional dependent "residual" (or warping) displacements of the beam. The in-plane functions ψ_x and ψ_y, which are associated with formation of the anticlastic surface, can be neglected by assuming $\sigma_{xx} = \sigma_{yy} = \tau_{xy} = 0$ and thus, using a one-dimensional constitutive model,

$$\sigma_{zz} = E\epsilon_{zz} = E\left(\frac{\partial W}{\partial z} - x\frac{\partial \Phi_y}{\partial z} + y\frac{\partial \Phi_x}{\partial z}\right) \tag{18a}$$

$$\tau_{yz} = G\gamma_{yz} = G\left(x\frac{\partial \Theta}{\partial z} + \frac{\partial V}{\partial z} + \Phi_x + \frac{\partial \psi_z}{\partial y}\right) \tag{18b}$$

$$\tau_{xz} = G\gamma_{xz} = G\left(-y\frac{\partial \Theta}{\partial z} + \frac{\partial U}{\partial z} - \Phi_y + \frac{\partial \psi_z}{\partial x}\right) \tag{18c}$$

If one assumes that U, V, and W and Φ_x, Φ_y, and Θ represent the displacements and rotations about the centroid,[9] then the corresponding definition of the one-dimensional out-of-plane warping function [from Eq. (16c)] is

$$\psi_z = \psi(x, y) - b_4 x - b_5 y \tag{19}$$

where ψ is given in Eq. (7).

Alternatively, based on the work of Ref. 10, one can assume that U, V, and W and Φ_x and Φ_y are the mean displacements and the mean rotations of the cross section

$$U = \frac{1}{A}\int_A u\, dA \tag{20a}$$

$$V = \frac{1}{A}\int_A v\, dA \tag{20b}$$

$$W = \frac{1}{A}\int_A w\, dA \tag{20c}$$

$$\Phi_x = \frac{1}{I_{xx}} \int_A yw \, dA \tag{20d}$$

$$\Phi_y = -\frac{1}{I_{yy}} \int_A xw \, dA \tag{20e}$$

and the correct form of the out-of-plane warping is obtained by substituting Eq. (16c) into Eqs. (20a–20e) and then into Eq. (17c):

$$\psi_z = \psi - \frac{y}{I_{xx}} \int_A y\psi \, dA - \frac{x}{I_{yy}} \int_A x\psi \, dA - \frac{1}{A} \int_A \psi \, dA \tag{20f}$$

where ψ is given in Eq. (7).

The development of the equations of motion and the corresponding boundary conditions using the kinematic relations of Eqs. (17a–17c) can be determined using Hamilton's principle, where the bending and torsion related section constants are dependent on the one-dimensional out-of-plane warping function ψ_z. The complete details of this refined model can be found in the second part of this paper.[11]

Finally, a set of linear equations can be developed that relates the kinematic description of shear strain and twist rate to the shear (P_x, P_y) and torsion (M_z) resultants, which can be used to 1) transform the warping function definition [Eq. (7)] to a kinematically scaled function, and 2) provide valuable one-dimensional cross-sectional constants. Substituting Eqs. (18b) and (18c) into Eqs (1a–1c) and carrying out the integration over the cross-sectional results in

$$\begin{bmatrix} R_{11} & R_{12} & 0 \\ R_{21} & R_{22} & 0 \\ R_{31} & R_{32} & 1 \end{bmatrix} \begin{bmatrix} P_x \\ P_y \\ M_z \end{bmatrix} = \begin{bmatrix} S_{11} & 0 & S_{13} \\ 0 & S_{22} & S_{23} \\ 0 & 0 & S_{33} \end{bmatrix} \begin{bmatrix} \dfrac{\partial U}{\partial z} - \Phi_y \\ \dfrac{\partial V}{\partial z} + \Phi_x \\ \dfrac{\partial \Theta}{\partial z} \end{bmatrix} \tag{21}$$

where the coefficients R_{ij} and S_{ij} are defined in the Appendix. Multiplying Eq. (21) by the inverse of R results in the following set of linear equations:

$$\begin{bmatrix} P_x \\ P_y \\ M_z \end{bmatrix} = \begin{bmatrix} GAk_{11} & GAk_{12} & -GA\bar{y}k_{13} \\ GAk_{12} & GAk_{22} & GA\bar{x}k_{23} \\ -GA\bar{y}k_{13} & GA\bar{x}k_{23} & GJ \end{bmatrix} \begin{bmatrix} \dfrac{\partial U}{\partial z} - \Phi_y \\ \dfrac{\partial V}{\partial z} + \Phi_x \\ \dfrac{\partial \Theta}{\partial z} \end{bmatrix} \tag{22}$$

where k_{11}, k_{12}, and k_{22} are the shear correction coefficients needed for Timoshenko's beam theory,[9] and k_{13} and k_{23} are the shear correction coefficients for coupling between flexure and torsion. This approach for flexure-torsion behavior is an extension of the method developed in Ref. 10 for uncoupled bending only.

Solution Procedure

Warping Function Determination via Power Series

The warping function ψ of Eq. (7), which is dependent on both the cross-sectional shape as well as the material properties, can be determined by solving a set of variationally derived algebraic equations based on the principle of minimum potential energy. In this development, the warping function is defined as a power series:

$$\psi(x, y) = \sum_{m=0}^{\infty} \sum_{n=0}^{\infty} c_{mn} x^m y^n - c_{00} \tag{23}$$

where c_{mn} are the unknown coefficients and the rigid-body translation coefficient c_{00} is not included since it was accounted for in Eq. (3c) by b_3. If one assumes a finite series, then the previous equation can be written in matrix form as

$$\psi(x, y) = [N(x, y)](c) \tag{24}$$

where $N(x, y)$ is an array of the power terms, c is an array of unknown coefficients, and the array sizes are dependent on the selected polynomial order. For example, if a cubic polynomial was selected, then based on Pascal's triangle there are nine terms, and the previous arrays have the form

$$[N(x, y)] = [x, y, x^2, xy, y^2, x^3, x^2y, xy^2, y^3] \tag{25a}$$

$$(c)^T = [c_{10}, c_{01}, c_{20}, c_{11}, c_{02}, c_{30}, c_{21}, c_{12}, c_{03}] \tag{25b}$$

A set of linear algebraic equations for determining the coefficients c can be obtained by substituting Eq. (24) into Eq. (6) and taking the variation with respect to the unknown coefficients ($\delta\psi = [N(x, y)]\{\delta c\}$):

$$[K](c) = [[F_w] - [F_c]](Q) \tag{26a}$$

where the stiffness matrix is defined as

$$[K] = GL \int_A \frac{\partial}{\partial x} [N(x, y)]^T \frac{\partial}{\partial x} [N(x, y)] + \frac{\partial}{\partial y} [N(x, y)]^T \frac{\partial}{\partial y} [N(x, y)] \, dA \tag{26b}$$

the force matrices are presented as

$$[F_w] = EL \left[\int_A x[N]^T \, dA, \int_A y[N]^T \, dA, 0 \right] \tag{26c}$$

$$[F_c] = GL \int_A \left[\frac{\partial}{\partial y} [N(x,y)]^T, \frac{\partial}{\partial x} [N(x, y)]^T \right] \times \begin{bmatrix} -\nu xy & -\dfrac{\nu}{2}(y^2 - x^2) & x \\ -\dfrac{\nu}{2}(x^2 - y^2) & -\nu xy & -y \end{bmatrix} dA \tag{26d}$$

and

$$(Q)^T = \left(\frac{P_x}{EI_{yy}}, \frac{P_y}{EI_{xx}}, \theta \right) \tag{26e}$$

The coefficients $c^{(1)}$ associated with the unit warping function ψ_1 in Eq. (7) are determined by setting $(Q)^T = \{1, 0, 0\}$. Similarly, the coefficients $c^{(2)}$ for ψ_2 and $c^{(3)}$ for ψ_3 are determined by performing analyses with $(Q)^T = \{0, 1, 0\}$ and $(Q)^T = \{0, 0, 1\}$, respectively. Thus, the complete warping function distribution for the three cases can be written in matrix form as

$$(\psi_1, \psi_2, \psi_3) = [N(x, y)]\{[c^{(1)}], [c^{(2)}], [c^{(3)}]\} \tag{27}$$

Computer Program

A computer program was written where, first, the boundary of a general cross section is defined using n coordinate points with n straight line segments connecting the points. Second, the cross section is discretized into n triangular subregions, where one edge of a triangle is a boundary line segment and the other two edges connect the endpoints of a boundary line segment with the user-defined cross-sectional origin. Thus all of the subregions have one corner that is defined at the origin. See Fig. 3b for an example of a rectangle defined using four triangular subregions. Third, the cross-sectional centroid and principal axes are calculated, and then the cross-sectional coordinates and applied forces are transformed to the cross-sec-

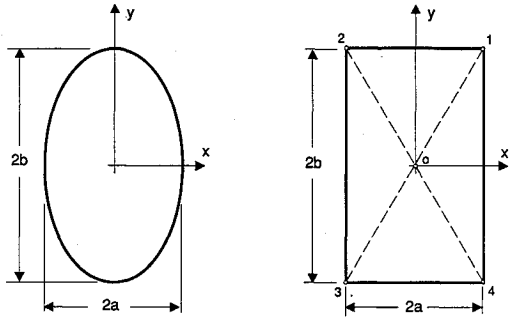

Fig. 3 Elliptical and rectangular cross sections with aspect ratio b/a; the rectangular cross section reveals the four triangular subregions.

tional principal axes. Fourth, the area integrals [Eqs. (26b-26d)] for each triangle subregion are evaluated using exact Gaussian quadrature formulas,[8] where the cross-sectional power series polynomial can be user defined. Fifth, the complete cross-sectional stiffness and force matrices are formed by simply adding together (not finite element type assembling) all of the triangular subregion matrices. Sixth, the coefficients for each of the three cases of Q are determined. Seventh, the calculated coefficients along with the power series polynomial definition are used to determine the shear stress distribution and the cross-sectional properties (shear center location, torsion constant, shear correction factors, etc.). Finally the calculated values are transformed from the cross-sectional principal axes back to the user-defined coordinate system.

This approach strongly differs from previous finite element based approaches[4,5] in that the global matrix size is defined by the assumed polynomial order and not the complexity of the cross section. Moreover, cross-sectional cavities can be easily treated by simply subtracting off the triangular subregions that define the cavity. The aspect ratio of a triangle subregion is not critical, since the power series is a global cross-sectional function and not a local subregion function (i.e., finite element method).

Numerical Results

Prismatic cantilever beams with three different types of cross sections are studied first to verify the current approach (ellipse, rectangle), Fig. 3, and second to illustrate important results not found in the literature (NACA four-digit airfoils), Fig. 4. The beam material properties are defined as $E = 1.0$ and $\nu = 0.333$.

Ellipse

Initially the current approach was verified by studying the behavior of cantilever beams with elliptical cross sections having a wide range of aspect ratios ($0.01 \le b/a \le 100$), where a and b are the semi-axes length in the x and y directions, respectively. See Fig. 3a. Each elliptical cross section was discretized using 90 points on the cross section (i.e., 90 triangular subregions), and the warping functions were defined using a cubic polynomial (nine unknown coefficients) with a corresponding exact Gaussian quadrature formula.[8] In Fig. 5, the variation of the nonzero nondimensionalized coefficients for an applied bending curvature rate P_x/EI_{yy} and twist rate θ are presented as a function of aspect ratio b/a, where the circles are the current calculated power series solution and the bold solid lines are the exact solution from Ref. 2. The flexure solution in the x direction is composed of only three nonzero terms ($\psi_1 = c_{10}x + c_{12}xy^2 + c_{30}x^3$), where the remaining six calculated coefficients are equal to zero. The c_{10} term is proportional to the shear strain at the beam root $\gamma_{xz(0)}$ and thus is used as a measure of shear deformation in the x direction (b_4), from Eq. (15a):

$$\frac{c_{10}}{a^2} = \frac{1}{a^2}\frac{\partial \psi_1}{\partial x}\bigg|_{x=y=0} = \frac{\gamma_{xz_{(0)}} EI_{yy}}{a^2 P_x} = \frac{b_4 EI_{yy}}{a^2 P_x} \tag{28a}$$

Applying a force in the y direction, P_y, would produce only three nonzero coefficients, c_{01}, c_{21}, and c_{03}, where again the remaining six coefficients are equal to zero. The coefficient c_{01} is proportional to $\gamma_{yz_{(0)}}$ and represents a measure of shear deformation in the y direction (b_5):

$$\frac{c_{01}}{b^2} = \frac{1}{b^2}\frac{\partial \psi_2}{\partial y}\bigg|_{x=y=0} = \frac{\gamma_{yz_{(0)}} EI_{xx}}{b^2 P_y} = \frac{b_5 EI_{xx}}{b^2 P_y} \tag{28b}$$

The twist rate dependent warping function is composed of only the bilinear term ($\psi_3 = c_{11}xy$), where the remaining eight coefficients are equal to zero and c_{11} goes to zero as the cross section becomes a circle ($b/a = 1$). The torsion constant $GJ = a_3$ was calculated for each aspect ratio and was found to be in exact agreement (identical to eight decimal places) with the closed-form solution of Ref. 2:

$$GJ = G\pi \frac{a^3 b^3}{a^2 + b^2} \tag{29}$$

which was expected since the current torsion warping function is in agreement with the published solutions. The shear center was calculated and found to be coincident with the centroid for all aspect ratios ($x_s^* = x_s = 0$, $y_s^* = y_s = 0$). Finally, the shear correction factors k_{11} and k_{22} were calculated and compared with the results of Cowper[10] (see Table 1). The current predictions are in near exact agreement over a broad range of aspect ratios, where it is interesting to note that for a force acting through a very thin ellipse (for example, P_y with $b/a \approx 0$) the shear correction factor approaches zero, whereas for a force acting through a thick ellipse (P_x with $b/a \approx 0$) the shear correction factor approaches 0.917184.

Rectangle

The behavior of cantilever beams having rectangular cross sections was also studied to further validate the current approach. A wide range of aspect ratios ($0.01 \le b/a \le 100$) were investigated, where each cross section was discretized using the four corner points (four triangular subregions). See Fig. 3b. From Ref. 2, the exact solution of the x-dependent bending curvature rate warping function ψ_1 is defined as

$$\psi_1 = a^2\left[\frac{\nu}{3}\left(\frac{b}{a}\right)^2 - (1+\nu)\right]x - \left(\frac{\nu}{2}\right)xy^2 + \frac{1}{6}(2+\nu)x^3 + \frac{4\nu b^3}{\pi^3}\sum_{n=1}^{\infty}\frac{(-1)^n}{n^3}\frac{\sinh[n\pi(x/b)]}{\cosh[n\pi(a/b)]}\cos\left(n\pi\frac{y}{b}\right) \tag{30}$$

To compare the current power series predictions with the previous infinite series of transcendental functions, a Taylor series expansion was performed on Eq. (30) and the first three nonzero terms were found to be

$$\psi_1 \approx a^2\left[\frac{\nu}{3}\left(\frac{b}{a}\right)^2 - (1+\nu) + 4\nu S_{(-2)}\right]x - \frac{\nu}{2}[1 + 4S_{(0)}]xy^2 + \frac{1}{6}[2 + \nu + 4\nu S_{(0)}]x^3 + \cdots \tag{31a}$$

Table 1 Shear correction factors for elliptical cross sections ($\nu = 0.333$)

b/a	k_{11}	k_{11}, Ref. 11	k_{22}
0.01	0.917181	0.917181	0.004777
0.10	0.916854	0.916854	0.309770
0.20	0.915869	0.915869	0.602246
0.50	0.909272	0.909272	0.829613
1.00	0.888864	0.888864	0.888864
2.00	0.829613	0.829613	0.909272
5.00	0.602246	0.602246	0.915869
10.0	0.309770	0.309970	0.916854
20.0	0.105567	0.105567	0.917102
100.0	0.004777	0.004777	0.917181

Table 2 Calculated nonzero flexure and torsion power series coefficients, shear correction factor, and torsion constant for a square cross section (b/a = 1.00) with ($\nu = 0.333$)

Polynomial order	Matrix size	Flexure—x direction				Torsion	
		c_{10}/a^2	c_{30}	c_{12}	k_{11}	$c_{31}(-c_{13})$	k_t
2	5	0.8887	—	—	1.000	—	0.167
4	14	1.2405	−0.3888	0.1110	0.85105	1.556	0.141
6	27	1.2324	−0.3615	0.1018	0.85105	1.250	0.141
8	44	1.2340	−0.3690	0.1108	0.85105	1.574	0.141
Reference		1.2340	−0.3705	0.1114	0.85105	1.574	0.141

Table 3 Calculated nonzero flexure and torsion power series coefficients, shear correction factor, and torsion constant for a thin rectangular cross section (b/a = 100) with ($\nu = 0.333$)

Polynomial order	Matrix size	Flexure—x direction				Torsion	
		c_{10}/a^2	c_{30}	c_{12}	k_{11}	c_{11}	k_t
2	5	−554.0	—	—	1.000	1.00	0.333
4	14	0.7783	−0.3888	−0.1663	0.85105	1.00	0.333
6	27	1.2483	−0.1118	−0.1670	0.85105	1.00	0.333
8	44	1.1130	−0.2334	−0.1514	0.85105	1.00	0.333
Reference		0.9943	−0.2873	−0.1382	0.85105	1.00	0.333

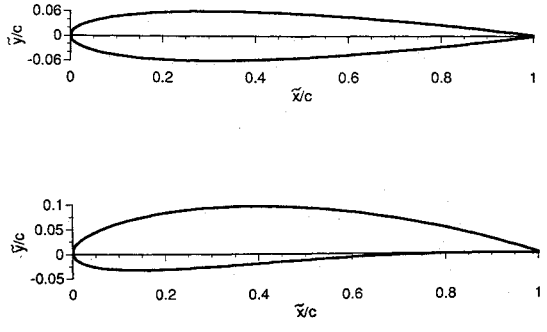

Fig. 4 a) NACA-0012 airfoil and b) NACA-4512 airfoil.

Table 4 Torsion coefficients k_t for rectangular cross sections ($\nu = 0.333$)

b/a	k_t	k_t, Ref. 2
1.00	0.14058	0.141
1.20	0.16613	0.166
1.50	0.19578	0.196
2.00	0.22871	0.229
2.50	0.24940	0.249
3.00	0.26336	0.263
4.00	0.28086	0.281
5.00	0.29137	0.291
10.00	0.31297	0.312
∞	0.33333	0.333

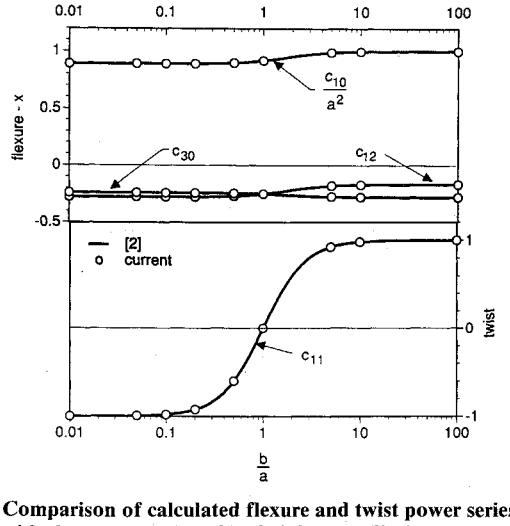

Fig. 5 Comparison of calculated flexure and twist power series coefficients with the exact results of Ref. 2 for an elliptical cross section.

where

$$S_{(i)} = \sum_{n=1}^{\infty} \frac{(-1)^n [n\pi(a/b)]^i}{\cosh[n\pi(a/b)]} \tag{31b}$$

The torsion rate warping function ψ_3 is also described by an infinite transcendental series,[2] but as b/a approaches either zero or infinity the series reduces to simply $\psi_3 = c_{11}xy$ with $c_{11} = -1$ or $c_{11} = 1$, respectively. Moreover, the torsion warping function for a square cross-section ($b/a = 1$) can be expressed using a Taylor series expansion as

$$\psi_3 \approx 1.574xy\left[\left(\frac{x}{a}\right)^2 - \left(\frac{y}{b}\right)^2\right] - 0.9021xy\left[\left(\frac{x}{a}\right)^4 - \left(\frac{y}{b}\right)^4\right] + 0.4909xy\left[\left(\frac{x}{a}\right)^6 - \left(\frac{y}{b}\right)^6\right] + 9.794xy\left(\frac{x}{a}\right)^2\left(\frac{y}{b}\right)^2\left[\left(\frac{x}{a}\right)^2 - \left(\frac{y}{b}\right)^2\right] + \cdots \tag{32}$$

The calculated torsion rate warping function ψ_3 is used to determine the torsion rigidity

$$GJ = a_3 = Gk_t(2a)^3(2b) \tag{33}$$

where k_t is the torsion constant.

Two cross-sectional aspect ratios ($b/a = 1,100$) were initially studied to assess the convergence of the calculated coefficients and the warping-dependent cross-sectional constants as a function of the polynomial order for the warping function. In Tables 2 and 3, the first three nonzero flexure coefficients, the first torsion coefficient, the shear correction factor, and the torsion constant are presented as a function of power series order and solution matrix size. In addition, reference values for the calculated values are presented, where the three flexure coefficients are determined using Eq. (31), the torsion coefficient is taken from Eq. (32), the shear correction factor k_{11} is taken from Ref. 10, and the torsion constant k_t is taken from Refs. 2 and 3. From these tables, it is obvious that the integrated cross-sectional constants converge to the reference

values much quicker than the actual power series coefficients. This occurs because the calculated coefficients represent a best-fit of the user-defined polynomial to the transcendental series, and changing the order of the polynomial will change the magnitude of the calculated coefficients, but it will have virtually no effect on the integrals of these functions. Thus, if one is only interested in warping related cross-sectional constants, then a low-order power series polynomial can be used, but if one is interested in the details of the warping function, then a much higher order polynomial is required.

In Fig. 6, the first three nonzero nondimensionalized power series flexure coefficients (symbols) are presented along with the Taylor series representation of Eq. (30) given by the bold solid lines. The power series solution produces near exact agreement over a broad range of aspect ratios ($0.01 \leq b/a < 100$), where a ninth-order polynomial (54 unknowns) was used for the warping function. As b/a approaches 100 (transversely loaded plate-type cross section), the power series predictions deviate from the Taylor series representation. This can be traced to the fact that the infinite transcendental series in Eq. (30) converges slowly for large b/a and the selected ninth-order polynomial cannot accurately represent this behavior. Thus, one would need to go to an even higher order polynomial for this severe aspect ratio. The shear center (x_s, y_s) and shear correction factors k_{11} and k_{22} were calculated for the entire range of aspect ratios, and it was found that the shear center was always located at the centroid and the shear correction factors were always equal to 0.85105, which is in exact agreement with Ref. 10 using $\nu = 0.333$. The calculated torsion constant k_t is presented in Table 4 as a function of aspect ratio, where the current results are in near perfect agreement with Ref. 2.

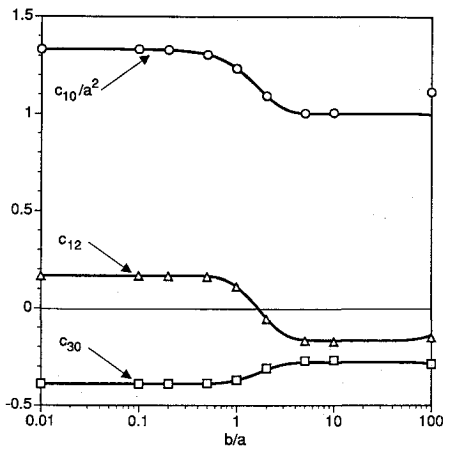

Fig. 6 Comparison of the first three nonzero calculated flexure power series coefficients with the Taylor series expansion of the results from Ref. 2 (—) for a rectangular cross section.

NACA Four-Digit Airfoils

The final set of beam cross sections that were investigated included six NACA four-digit airfoils of different thickness (NACA 0006, 0012, and 0018) and camber (NACA 2512, 4512, and 6512). The numbering system for these airfoils is based on section geometry,[19] where the first digit indicates the maximum value of the mean-line ordinate in percent of chord c, the second digit indicates the distance from the leading edge to the maximum camber location in tenths of chord, and the last two digits indicate the maximum thickness t_{max} in percent of chord. Two of the studied airfoils, NACA-0012 and NACA-4512, are presented in Fig. 4, where a second coordinate system $(\tilde{x}, \tilde{y})$ is introduced with the origin taken as the leading edge. Each airfoil was discretized using 95 points on the cross-section boundary (i.e., 95 triangular subregions), the warping functions were modeled using a ninth-order power series polynomial (54 unknown coefficients), and the numerical integration was performed exactly using a 52-point Gaussian quadrature formula.[8]

The calculated section properties for the six airfoils are presented in Table 5. The first five parameters represent the chord normalized geometric section constants and the sixth parameter β is the rotation angle from (x, y) to the principal axes (x, y) with counterclockwise defined as positive. The remaining nine parameters represent the torsion- and flexure-dependent values. The torsion coefficient k_t, which is nearly independent of airfoil thickness and camber, is found using the calculated torsion constant GJ:

$$GJ = a_3 = Gk_t(t_{max})^3 c \tag{34}$$

The chord normalized flexure dependent coefficients c_{10} and c_{01} are also presented and are used to provide a measure of chord-wise and thickness-wise shear deformation [see Eqs. (28a) and (28b)]. From the coefficient c_{10}, it is readily apparent that the application of a force in the chordwise direction P_x will produce nearly constant shear deformation regardless of airfoil thickness or camber, whereas the shear deformation associated with a thickness-wise force P_y is highly dependent on the airfoil thickness but only slightly dependent on camber. The shear center locations are also presented for the two definitions using the second coordinate system $(\tilde{x}, \tilde{y})$. Both definitions locate the shear center ahead of the centroid, where

Table 5 Section properties of NACA four-digit airfoils ($\nu = 0.333$)

	NACA-0006	NACA-0012	NACA-0018	NACA-2512	NACA-4512	NACA-6512
Centroid						
$\tilde{x}/c$	0.42067	0.42067	0.42067	0.42061	0.42039	0.42006
$\tilde{y}/c$	0.00000	0.00000	0.00000	0.01520	0.03037	0.04550
A/c^2	0.04106	0.08213	0.12319	0.08219	0.08238	0.08270
I_{xx}/c^4 (10^{-5})	0.84944	6.79550	22.9350	6.97050	7.49940	8.39180
I_{yy}/c^4 (10^{-3})	2.26500	4.52990	6.79490	4.53690	4.55840	4.59370
β, deg	0.00000	0.00000	0.00000	0.41351	0.82850	1.24740
k_t	0.15642	0.15386	0.14986	0.15396	0.15427	0.15479
c_{10}/c^2 (10^{-1})	1.89102	1.89302	1.89633	1.89609	1.90553	1.92117
c_{01}/c^2 (10^{-4})	8.15829	32.5947	73.1685	32.5100	32.2590	31.8141
$\tilde{x}_s/c$	0.33935	0.34093	0.34350	0.34399	0.35233	0.36402
$\tilde{y}_s/c$	0.00000	0.00000	0.00000	0.02183	0.04378	0.06595
$\tilde{x}_s^*/c$	0.36634	0.36711	0.36838	0.36871	0.37319	0.37985
$\tilde{y}_s^*/c$	0.00000	0.00000	0.00000	0.02196	0.04398	0.06614
k_{11}	0.91545	0.91462	0.91323	0.90181	0.86340	0.80324
k_{22}	0.07740	0.24212	0.40041	0.22576	0.19355	0.16671
U_D^*/U_D	0.87640	0.88120	0.89350	0.89100	0.91140	0.93710

the difference between the two definitions is nearly 50% (measured from the centroid with $\nu = 0.333$) in the x direction and a minimal amount in the y direction (cambered airfoils). It is interesting to note that the shear center moves rearward (closer to the centroid) by either increasing the thickness or camber. The difference that these two shear center locations have on the torsional divergence speed of a straight uniform aircraft wing can be studied using (from Ref. 20)

$$U_D = \frac{\pi}{2L}\sqrt{\frac{GJ}{cea_0(\rho/2)}} \tag{35}$$

where ρ is the air density, a_0 is the lift curve slope, and e is the distance from the elastic axis (line of shear centers) to the quarter-chord. The ratio of the divergence speed U_D^* using the corrected shear center location (aligned with the center of twist) based on Refs. 16 and 17 to the divergence speed U_D using the classical definition,[12] while holding everything else constant, is equal to

$$\frac{U_D^*}{U_D} = \sqrt{\frac{\theta}{e^*}} \tag{36}$$

where the results for the six different airfoil sections are given in Table 5. Thus it is apparent that the new (corrected) shear center location will predict divergence speeds that are significantly lower (6–12%) than those using the classic shear center definition, and this reduction is larger for thin airfoils with little or no camber.

Lastly, the shear correction factors k_{11} and k_{22} are presented. Increasing the airfoil thickness will produce a minor decrease in k_{11} but increase k_{22} significantly. This observation is in close agreement with the thin elliptical cross-sectional results (Table 1, $0.01 < b/a < 0.20$). Introducing camber will significantly reduce both shear correction factors k_{11} and k_{22}.

Conclusions

The flexure-torsion behavior of a tip-loaded cantilever beam with an arbitrary cross section is studied using Saint-Venant's semi-inverse method along with a power series solution for the out-of-plane flexure and torsion warping functions. The power series coefficients are determined by solving a set of variationally derived linear algebraic equations. For complex cross sections, the calculated coefficients represent a best-fit approximation to the exact warping function. A new linear relation is developed for locating the shear center using the Saint-Venant flexure and torsion solutions, where the twist rate is zero about the line of shear centers (not the centroidal axis). In addition, the kinematic relations for a fully compatible one-dimensional beam theory are presented, where the calculated current flexure and torsion warping functions are fully integrated into the development (see Ref. 11). Numerical results are presented for three different cross sections (ellipse, rectangle, and NACA four-digit airfoils). For elliptical cross sections, it was shown that the calculated coefficients, as well as all of the section properties, were in exact agreement with existing elasticity solutions. For the rectangular cross section, it was shown that the calculated power series coefficients represent a best-fit to the transcendental functions, and a low-order polynomial can be used if only warping-related section properties are desired, whereas a higher order polynomial is required if the warping function is to be studied in detail. Finally, for NACA four-digit airfoils, the shear deformation and shear correction factor associated with a thickness-wise force P_y is highly dependent on the airfoil thickness but only slightly dependent on camber. The x direction shear center location is ahead of the centroid with the difference in the two definitions being nearly 50% (for $\nu = 0.333$) when measured from the airfoil centroid, and increasing either the airfoil thickness or the camber will move the shear center closer to the centroid. These differences correspond to a 6–12% decrease in the divergence speed for the corrected shear center definition vs the classic definition.

Appendix

$$S_{11} = S_{22} = GA \tag{A1, A2}$$

$$S_{13} = G\int_A \left(\frac{\partial \psi_{z3}}{\partial x} - y\right) dA \tag{A3}$$

$$S_{23} = G\int_A \left(\frac{\partial \psi_{z3}}{\partial y} + x\right) dA \tag{A4}$$

$$S_{33} = G\int_A x\left(x + \frac{\partial \psi_{z3}}{\partial y}\right) - y\left(\frac{\partial \psi_{z3}}{\partial x} - y\right) dA \tag{A5}$$

$$R_{11} = 1 - \frac{G}{EI_{yy}}\int_A \frac{\partial \psi_{z1}}{\partial x} dA \tag{A6}$$

$$R_{12} = -\frac{G}{EI_{xx}}\int_A \frac{\partial \psi_{z2}}{\partial x} dA \tag{A7}$$

$$R_{21} = -\frac{G}{EI_{yy}}\int_A \frac{\partial \psi_{z1}}{\partial y} dA \tag{A8}$$

$$R_{22} = 1 - \frac{G}{EI_{xx}}\int_A \frac{\partial \psi_{z2}}{\partial y} dA \tag{A9}$$

$$R_{31} = -\frac{G}{EI_{yy}}\int_A \left(x\frac{\partial \psi_{z1}}{\partial y} - y\frac{\partial \psi_{z1}}{\partial x}\right) dA \tag{A10}$$

$$R_{32} = -\frac{G}{EI_{xx}}\int_A \left(x\frac{\partial \psi_{z2}}{\partial y} - y\frac{\partial \psi_{z2}}{\partial x}\right) dA \tag{A11}$$

Acknowledgments

The support of this research was provided by the NASA-Langley Research Center through Grant NAG-1-1151-FDP, with R. C. Lake as project monitor. The discussions and encouragement provided by E. Reissner are gratefully acknowledged.

References

[1]Love, A. E. H., *A Treatise on the Mathematical Theory of Elasticity,* 4th ed., Dover, 1944, pp. 310–348.

[2]Sokolnikoff, I. S., *Mathematical Theory of Elasticity,* 2nd ed., McGraw-Hill, New York, 1956, pp. 104–220.

[3]Timoshenko, S. P., and Goodier, J. N., *Theory of Elasticity,* 3rd ed., McGraw-Hill, New York, 1970, pp. 291–313, 354–374.

[4]Herrmann, L. R., "Elastic Torsional Analysis of Irregular Shapes," *ASCE Journal of Engineering Mechanics Division,* Vol. 91, No. 1, 1965, pp. 11–19.

[5]Mason, W. E., and Herrmann, L. R., "Elastic Shear Analysis of General Prismatic Beams," *ASCE Journal of Engineering Mechanics Division,* Vol. 94, No. 6, 1968, pp. 965–983.

[6]Mindlin, R. D., "Solution of St. Venant's Torsion Problem by Power Series," *International Journal of Solids and Structures,* Vol. 11, No. 4, 1975, pp. 321–328.

[7]Cowper, G. R., "Gaussian Quadrature Formulas for Triangles," *International Journal for Numerical Methods in Engineering,* Vol. 7, No. 6, 1973, pp. 405–408.

[8]Dunavant, D. A., "High Degree Efficient Symmetrical Gaussian Quadrature Rules for Triangle," *International Journal for Numerical Methods in Engineering,* Vol. 21, No. 12, 1985, pp. 1129–1148.

[9]Timoshenko, S. P., "On the Correction for Shear of the Differential Equations for Transverse Vibrations of Prismatic Beams," *Philosophical Magazine,* Vol. 41, No. 8, 1921, pp. 744–746.

[10]Cowper, G. R., "The Shear Coefficient in Timoshenko's Beam Theory," *ASME Journal of Applied Mechanics,* Vol. 33, No. 2, 1966, pp. 335–340.

[11]Kosmatka, J. B., "Flexure-Torsion Behavior of Prismatic Beams, Part II: A Compatible Shear Deformable One-Dimensional Theory," *AIAA Journal* (to be published).

[12]Griffith, A. A., and Taylor, G. I., "The Problem of Flexure and its Solution by the Soap-Film Method," *Reports and Memoranda of*

Advances and Communications in Aeronautics, Vol. 1, No. 399, 1917, pp. 1–6.

[13]Stevenson, A. C., "Flexure with Shear and Associated Torsion," *Philosophical Transactions of the Royal Society,* Vol. 237, No. 2, 1939, pp. 161–229.

[14]Goodier, J. N., "A Theorem on the Shearing Stress in Beams," *Journal of the Aeronautical Sciences,* Vol. 11, No. 2, 1944, pp. 272–280.

[15]Duncan, W. J., "The Flexural Centre of Centre of Shear," *Journal of the Royal Aeronautical Society,* Vol. 57, No. 8, 1953, pp. 594–597.

[16]Reissner, E., "The Center of Shear as a Problem of the Theory of Plates of Variable Thickness," *Ingenieur-Archiv,* Vol. 59, No. 4, 1989, pp. 324–332.

[17]Reissner, E., "Approximate Determinations of the Center of Shear by Use of the Saint-Venant Solution for the Flexure Problem of Plates of Variable Thickness," *Archive of Applied Mechanics-Ingenieur-Archiv,* Vol. 61, No. 8, 1991, pp. 555–566.

[18]Jacobs, J. A., "The Centre of Shear of Aerofoil Sections," *Journal of the Royal Aeronautical Society,* Vol. 57, No. 3, 1953, pp. 235–237.

[19]Abbott, I. R., and Von Doenhoff, A. E., *Theory of Wing Sections,* 1st ed., Dover, New York, 1959, pp. 111–115.

[20]Bisplinghoff, R. L., Ashley, H., and Halfman, R. L., *Aeroelasticity,* 2nd ed., Addison-Wesley, Reading, MA, 1955, p. 432.